Assessment and Estimation on Operation Range of Experimental Unmanned Helicopter

Hoang Thi Kim Dung

Hanoi University of Science and Technology, Ha Noi, Vietnam
Corresponding author email: dung.hoangthikim@hust.edu.vn

Abstract

The object of the study is to research a Helicopter Unmanned Aerial Vehicle (HUAV) made by bilateral project HNQT/SPĐP/12.19 at Hanoi University of Science and Technology. The purpose is to study the effect of the experimental set on the aerodynamic characteristics of this unmanned helicopter and study the phenomenon of aerodynamic elasticity to provide an assessment of the durability of the model in the hovering flight mode. The one-way fluid structure interaction (FSI) method which is a combination of Computational Fluid Dynamics (CFD) and Computational Structural Dynamics (CSD), has been carried out to comprehend both aerodynamic and aeroelasticity phenomena of HUAV. The CFD results show the distribution of pressure, velocity, and turbulence in accordance with the actual phenomenon. The CSD results show displacements, stress distributions, and material limit assessments. Then, a suitable operating range that meets the feasibility and possibility of flight is created. This study is a premise for further experimental studies in the process of creating a HUAV.

Keywords: Aerodynamic, CFD, CSD, FSI, HUAV, hovering flight mode.

1. Introduction

In recent years, the application of unmanned aerial vehicles (UAVs), including unmanned helicopters (HUAV), has become more diverse in both civilian and military applications since UAVs are easier and faster to deploy than most other alternatives. There has been much numerical research about HUAV, but it seems to stop at separate simulations of each part of HUAV, such as the main rotor blade or body [1-11]. The study of the entire helicopter model is difficult because of i) the complexity of the model and the mesh requirements; ii) the relative motion between the rotating motion of the rotor and the stationary motion of body which requires complex handling methods. Two main methods to solve the above problem include constructing overlapping grids [2] or sliding grids [3].

Many studies have been carried out related to solving the above difficulties. Renaud *et al.* [4] provided a method compared with experimental measurements for the Dauphin 365 N model, excluding the tail rotor. The entire BO105 miniature model in the wind tunnel air duct was simulated by Khier [5]; or evaluated studies on the DLR and ONERA meshing grids by Sidès [1]; or simulation research of two main rotors and body [6]; or research in the wind tunnel [7, 8]. Biava and colleagues [9] have carried out studies on the model combined with the experiment. However, these studies have not mentioned the durability and material parameters of the experimental set as well as the model.

2. Objective Model and Methodology

2.1. Helicopter Unmanned Aerial Vehicle Model

A classical HUAV was built with a mass of 4N for the purpose of serving research and teaching. The main parts of HUAV model included wing assembly, the body and the base unit (Fig. 1).

Fig. 1. HUAV model

The main rotor assembly included blades and the root. The blade was rectangular with a size of 0.402 m x 0.075 m and NACA0015 profile. The blade structure provided nine wood ribs of 2 mm thickness to increase the resistance to distortion and denting of the blade. The skin of blade was made of wood within of

2 mm thickness to help ensure the aerodynamic properties of the model. There was an aluminium spar from the root to the tip of blade to enhance the durability of the blade. The root of blade often had the highest stress, which required high rigidity materials such as steel.

The HUAV model (Fig. 2) was redesigned with a body of composite materials and a plastic rotating disc. The base was designed with a fixed pillar that was made of steel. The base was positioned at the rear of the body to reduce the influence of aerodynamics on the flow properties. It was connected to the body structure through a composite rod. The properties of materials are in Table 1 and Table 2.

In this research, the HUAV model was performed with pitch angle from 9 to 12 degrees and rotational speeds from 650 to 850 rpm.
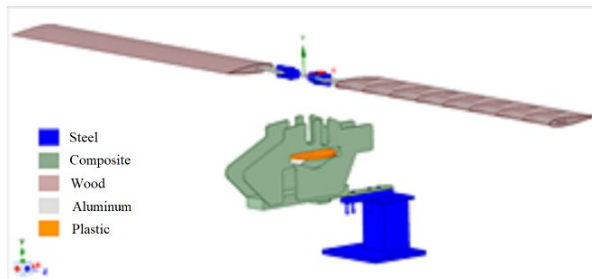

Fig. 2. Design HUAV model

Table 1. Properties of isotropic materials

Material	Tensile Yield Strength [MPa]	Compressive Yield Strength [MPa]
Wood	41	66.3
Aluminum	280	310
Steel	250	460

Table 2. Properties of composite materials

Direction	Critical strength [MPa]	Critical deformation [m/m]
X	34	0.0026
Y	1632	0.0143
Z	34	0.0026

The aerodynamic and structural properties of this blade were estimated by both Computational Fluid Dynamics (CFD), fluid structure interaction (FSI) and the modal method with the help of ANSYS software. Firstly, the CFD problem was solved to determine aerodynamic properties, including pressure distribution (or aerodynamic loads) on the turbine blade. Secondly, the deformation caused by aerodynamic loads on turbine blades was estimated by solving one-way FSI problem.

2.2. Methodology

Conservation equations are generated to describe the fluid flow in nature. These equations include the conservation of mass (continuous equation), the conservation of momentum (or Navier-Stokes equation), and the conservation of energy [10]. With two equations of continuity and Navier-Stokes for the incompressible flow, we get a system of four equations consisting of six unknowns. Different computational models are performed to solve this system of equations, such as DNS (Direct Numerical Simulation), LES (Large Eddy Simulation), and RANS (Reynold Averaged Navier-Stokes Simulation). RANS turbulence models are preferred to be used over other models thanks to their low error and especially saving computer performance, which, the continuity and Navier-Stokes equations are written as average equations. Then, turbulence models are used to model the tenser of Reynold stress. There are from one to seven equations, depending on the type of selected turbulence model.

Structural dynamics studies the behaviour of structures under the action of loads. Loads acting on the structure can be divided into two main categories: static loads and transient loads. The finite element method is used to solve for the motion of the structural kinematics that is described by [11]. This is a method of using approximation of differential equations by discretizing, dividing the complex continuum into simple domains, and connecting each other through nodes.

The FSI problem is a combination of aerodynamics (CFD) and structural dynamics (CSD) problems. Once the aerodynamic and structural equations have been built, the solution of this system of equations can be done by specialized calculation software. The one-dimensional FSI model is a combination of Fluent and the Mechanic Structure in ANSYS software. Results from Fluent are transferred to the Mechanic Structure for calculation.

In the study of flow for helicopters, the relative motion between the body and the rotor complicates the problem. Steijl and Barakos [3] developed a sliding mesh method to solve this problem. A sliding surface between the rotating area containing the rotor and the static area containing the body was created. The sliding surface allowed the transmission of aerodynamic properties between the two zones, which happened even when the two sides were not similar in terms of the mesh node and the mesh surface [3].

3. Simulation Setup

3.1. Computational Domain

The construction of the computational domain is one of the important issues that determines the results of the simulation problem. In order to perform simulation

computation, the simulation space domain must be large enough to avoid interference from the boundary layer on the entire aircraft.

For HUAV, the simulation domain is divided into two main regions, the rotation domain (containing the propeller blades) and the static domain (containing the body and base) for the purpose of modelling the rotation of the model.

The rotational domain is a round cylinder with dimensions of $1.1D$ x $0.0517D$ (Fig. 2a), where D is diameter of rotor, which has been studied previously. The 10D x 10D x 8D rectangular box-shaped static domain (Fig. 2b) is large enough to avoid disturbances from the boundary layer. The rotational and static domains are connected through interfaces, allowing for precise aerodynamic pressure transmission.

a. Rotational domain

b. Static domain

Fig. 2. Computational domain

3.2. Meshing Grid

The meshing aims to divide the computational element; it directly affects the simulation results. Therefore, the grid survey cannot be ignored. For the CFD simulation problem, the mesh requirements include: i) Ensuring the geometry of the object: the meshing is too coarse, causing the change of model's contours, which happens at positions with great curvature, such as the leading edge of the rotor blade; ii) ensuring mesh shape: the mesh distortion makes the simulation low accuracy. Therefore, quality control indicators are included (Orthogonal – orthogonal index, Skewness – standard deviation index). For Fluent simulation in Ansys, the Orthogonal index must be at least 0.01 to ensure the accuracy of the problem; iii) Boundary layer grid: The boundary layer mesh

allows the simulation to catch vortexes, the $y+$ index is less than 1 for $k\text{-}\omega$ turbulence models, and the $y+$ index is less than 200 for $k\text{-}\varepsilon$ turbulence models; iv) The number of grid elements, which affects the computation time of the model.

From the above grid requirements, the survey grid cases include:

1. Automatic meshing,

2. Face sizing 3mm on the wing face,

3. Split the wing face into different parts, face sizing 1mm in front, face sizing 3 mm in back,

4. Same as case 3 and add 0.3 mm inflation on the wings,

5. Splitting blocks for meshing purposes, like dividing ICEM tools in ANSYS software,

6. Same as case 3 and add 0.01 mm inflation on the wings,

7. Same as case 3, use inflation 0.01 mm,

8. Same as case 5 and using 0.01 mm inflation, face sizing 0.5 mm front faces, face sizing 1 mm back faces,

9. Same as case 5, use inflation 0.01 mm, face sizing 0.5 mm front faces, face sizing 0.5 mm back faces.

3.3. Boundary Conditions

For the aerodynamic problem (CFD problem) at hovering flight:

- Inlet: pressure inlet and set the Gauss pressure to 0 (equivalent to an absolute pressure of 1atm),

- Outlet: pressure outlet and set Gauss pressure to 0 (equivalent to absolute pressure of 1atm),

- Wall: include wings, body, and base. The main rotor is rotational area around the y axis with the centre of rotation at coordinates $(x, y, z) = (0, 0, 0)$ and rotation speed from 650 to 850 rpm. The interface faces are coupled together, allowing the pressure definition on the overlapping faces to be the same.

For the structural problem (CSD), the aerodynamic pressure is converted directly to the input condition for the structural problem, which is characteristic of the FSI problem (Fig. 3).
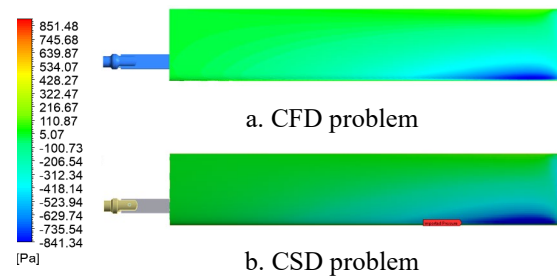

a. CFD problem

b. CSD problem

Fig. 3. Distribution of pressure on rotor blade

Other boundary conditions of the CSD problem include acceleration of gravity 9.81 m/s^2 in the *y* direction, rotational speed of the wing assembly, and wing root equal to the velocity in aerodynamic simulation, using the mount at the base, using remote displacement allows the wing root to be fixed while rotating. Unlike the problems that only simulate the wing, the simulation of the body requires a coherent relationship between the body and the wing (Fig. 4). A remote force is used to act directly on the bottom of the body with a magnitude equal to the lift on the wing calculated from the CFD problem (Fig. 5).

a. CFD

b. CSD

Fig. 4. Distribution of pressure on body and base

Fig. 5. Position of remote force

4. Results and Discussion

4.1. Effect of Meshing Grid

The effect of meshing grid is resumed in Table 3, Fig. 6, and Fig. 7.
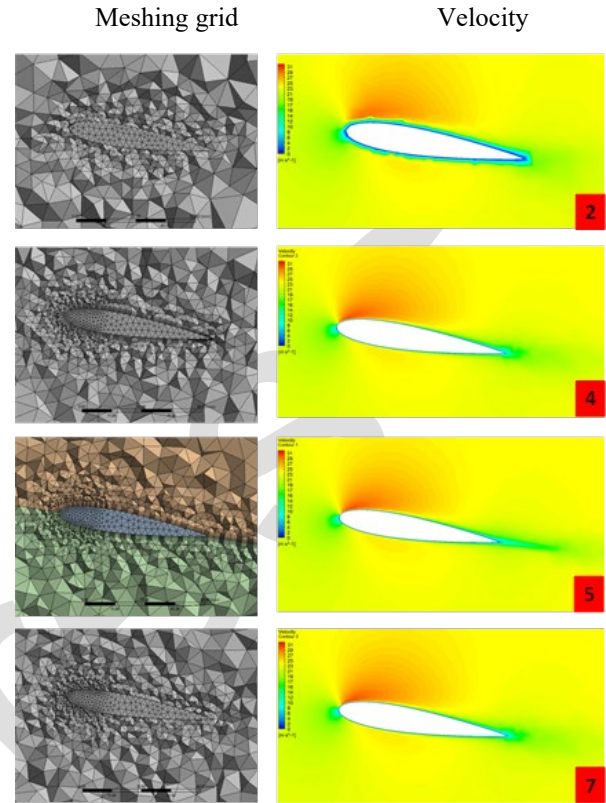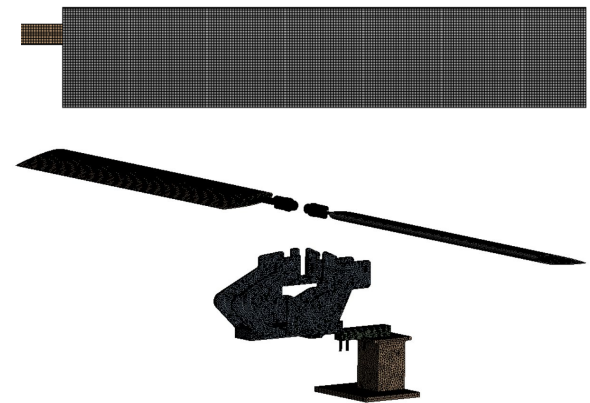

Fig. 6. Meshing grid and distribution of velocity

Fig. 7. Meshing grid of the structure problem

For cases 1, 2, and 3, the mesh is judged to be too coarse, affecting the geometry of the model at the leading edge of the wing and causing lift deviation. Using inflation in case 4 gives a good value in terms of *y+* but reduces the quality of the mesh shape. The block division in case 5 allows for ensuring the mesh shape, mesh quality, and boundary layer mesh value. This is a suitable model for pre-calculation.

Table 3. Effect of meshing grid

No	Elements	Nodes	Min. Orthogonal number	Max. Skewness number	y^+	Lift (N)	Error (%)
1	111003	19413	0.201	0.799	375.93	4.81	4.5
2	437847	79422	0.201	0.799	248.06	4.63	0.5
3	1681436	304647	0.2007	0.7993	90.9	4.63	0.7
4	1659156	454970	0.0997	0.8994	29.03	4.71	2.36
5	1849394	496566	0.0627	0.9373	55.05	4.56	0.81
6	2120474	532150	0.0029	0.9288	0.6	4.05	12.06
7	2120474	532150	0.0029	0.9288	0.41	4.8	4.37
8	8832507	2347900	0.0084	0.9329	0.4	4.72	2.53

For the cases with boundary layer *y+* less than 1 (cases 7, 8, 9), in order to achieve the quality of mesh geometry, the number of elements is too large, affecting the computation time. Therefore, the research scope is limited to the *k-ε* turbulence model in case 5.

For structural problems, the simple shaped wing surface is square meshed, while the complex framed body and base are meshed tetrahedral (Fig. 7).

4.2. Effect of Body and Base

With a factor of safety of 1.3, the required lift is 5.1 N. When increasing the pitch angle or increasing the rotational speed of main rotor, the drag force increases (Fig. 8). This is completely consistent with computational theory and practice. At a pitch angle of 9 degrees and a rotational speed of less than 700 rpm, the generated lift does not meet the requirements. Other cases completely meet the lifting force requirements (Fig. 8). This shows the feasibility of the model. Compared with the theoretical calculation results, the error for this simulation is always less than 12.12% (Table 4).

Thus, the correctness and reliability of the simulation process is checked by calculated the lift force. This difference is significant, approximately 11% for each case. This is explained by that the HUAV's body has created vortices which affect the aerodynamics, thereby creating shape resistance for this model. To be able to see more clearly the aerodynamics properties of the model, the 10-degree, 750 rpm case is analysed in detail (Fig. 9).

As the main rotor rotates, it creates a pressure differential region. Positive pressure in the area below the plane of rotation, and negative pressure occurs at the surface above the plane of rotation. Due to the pressure difference between the two blades, the air flow is sucked from the top down, through the rotating plane of the propeller, and then pushed down, creating traction for the aircraft. At the tip of the wing, swirls appear; these are basic features for the aerodynamic properties of the helicopter.

Table 4. Change of thrust with body and base (%)

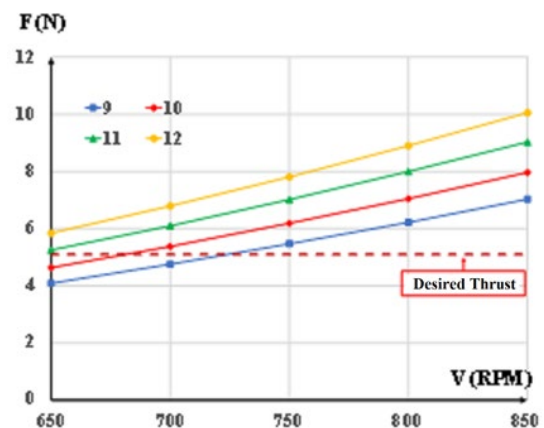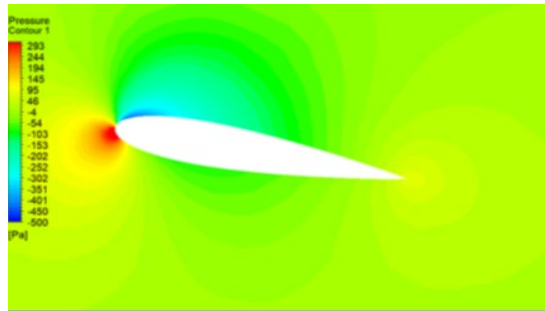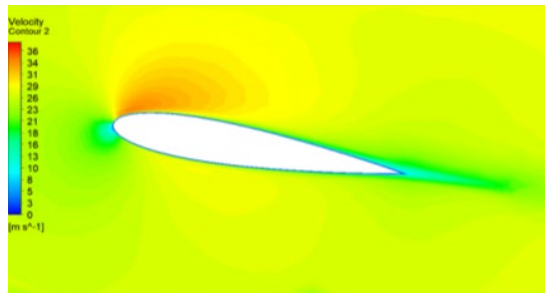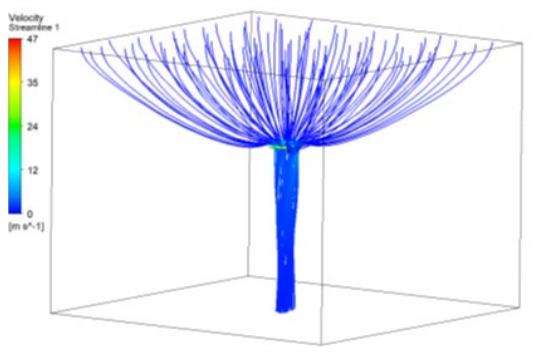| Attack angle (°)	Rotational speed (RPM)				
	650	700	750	800	850
9	10.05	9.78	9.94	10.11	10.03
10	11.96	12.12	11.86	11.87	11.86
11	10.34	11.59	11.52	11.49	11.47
12	11.80	11.87	11.84	11.82	11.83

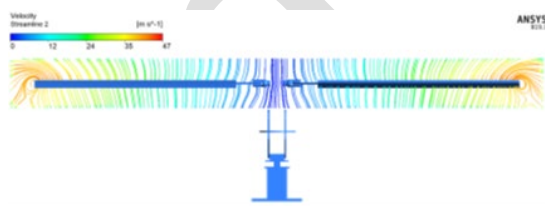Fig. 8. Thrust on the entire HUAV model

a. Pressure
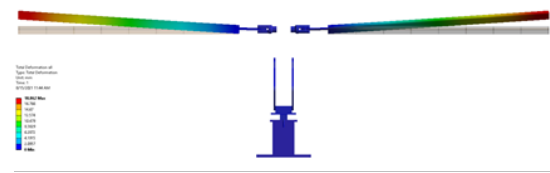

b. Velocity

c. Streamline

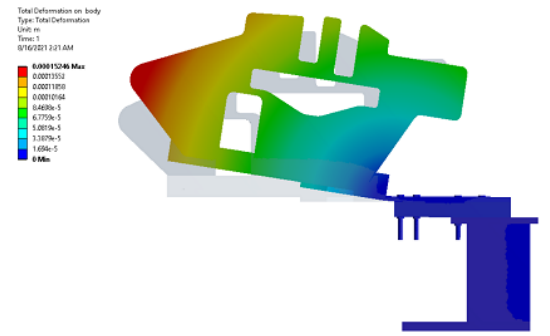d. Vortex at the tip of the main rotor blade

Fig. 9. Distribution of pressure and velocity

4.2. Strength Analysis

In general, the greatest displacement occurs at the tip of the wing (Fig. 10a). The root wings and the body of the HUAV have little displacement. The base region is almost non-displaced (Fig. 10b).

a. General

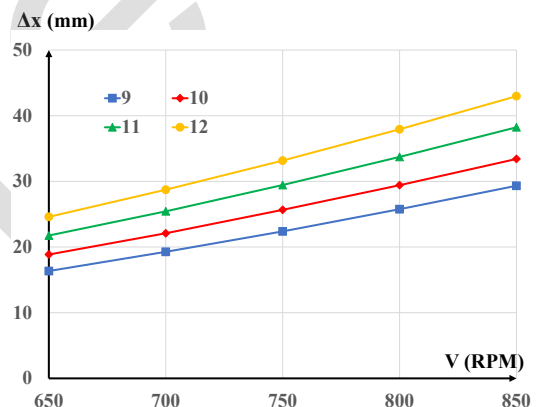

b. On body and base

Fig. 10. Displacement of HUAV

Fig. 11. Maximum displacement on HUAV

The cause of displacement comes from the aerodynamic forces acting on the wings and the entire body of the model. Therefore, the displacement characteristics of the model tend to change according to the aerodynamic characteristics when changing the pitch angle and rotational speed (Fig. 11).

This model does not use a single material, different materials have different strength limits that require surface studies to follow material regions. The factor of safety used for this study is 1.3.

When increasing the pitch angle or increasing the rotational speed of main rotor, the maximum stress increases (Fig. 12). All the maximum stress values for wood, steel, and composite materials are less than the critical stress of the material. Only the area of aluminium material corresponding to the crossbar connecting the base of the wing and the blade is in the danger zone (Fig. 13).
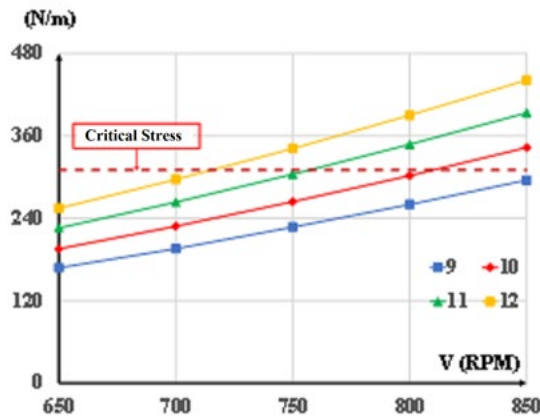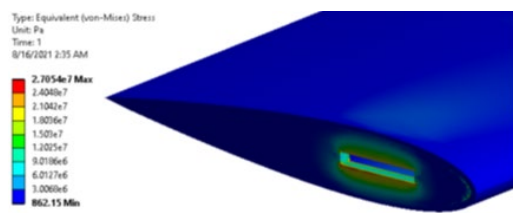
46

Fig. 12. Equivalent stress of aluminium areas

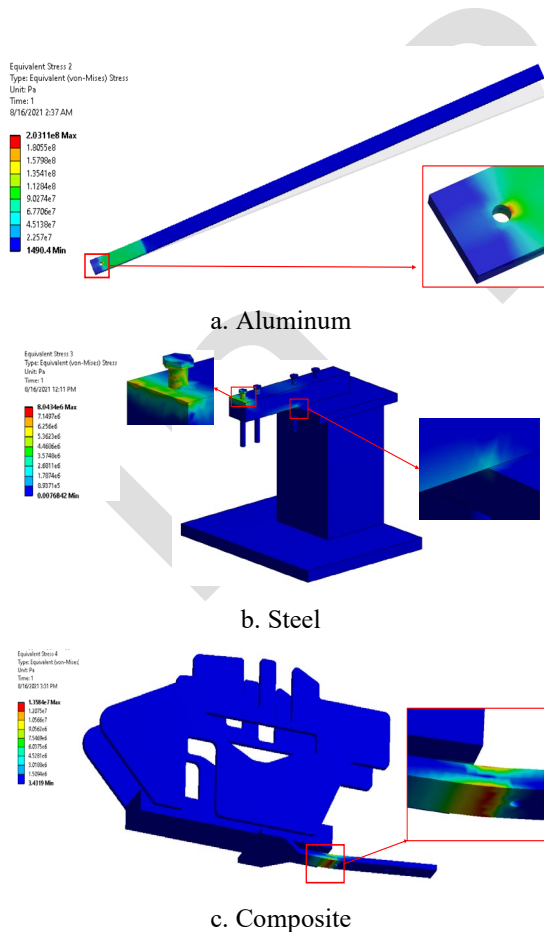Fig. 13. Distribution of equivalent stress on aluminium material

a. Aluminum

b. Steel

c. Composite

Fig. 14. Position of maximum equivalent stress

Table 5. Range of operation for HUAV

Attack angle (º)	Rotational speed (RPM)
9	730-850
10	680-800
11	660-750
12	650-720

For the blade pitch of 9 degrees, all cases satisfy the material's critical stress. Other pitch angles require a limit on the rotational speed. For example, the rotational speed is less than 800 rpm, 750 rpm, and 720 rpm at pitch angles of 10 degrees, 11 degrees, and 12 degrees, respectively. This is the upper limit of the survey procedure for this model.

The position of the maximum stress for each material region is presented in Fig. 14 for the case of 10 degrees, 750 rpm.

From the analysis of aerodynamic and material surveys, the study obtained the operating range for the HUAV model to ensure the feasibility and safety (Table 5).

5. Conclusion

This study aims to find out the influence of the body and based on the aerodynamic characteristics of the helicopter model. The study is carried out by calculating the one-way FSI simulation method through aerodynamic and structural calculations on the wings.

The simulation problem has an error of less than 7%. The simulation results show that, when increasing the pitch angle or rotational speed, the lift force increases as well as the stress displacements acting on the wings, body, and base.

The body and base create swirls that increase the aerodynamic drag of the model. Lift is reduced by almost 11% due to the influence of the body on the propeller blades.

The maximum displacement takes place at the tip of the wing, the other displacements are insignificant. The stresses in the different material regions all satisfied the critical stress value. Only the stress at the junction between the blade and the root of the blade is limited by the rotational speed. Since then, the operating range for the HUAV model to ensure the feasibility and safety has been estimated.

Acknowledgments

Inc. for the authorization to use ANSYS software in simulation works.

References

[1] J. Sidès, K. Pahlke and M. Costes, Numerical simulation of flows around helicopters at DLR and ONERA, Aerospace Science and Technology, vol. 5, issue 1, pp. 35–53, Jan. 2001.
https://doi.org/10.1016/S1270-9638(00)01078-6

[2] J. A. Benek, P. G. Buning and J. L. Steger, A 3-D chimera grid embedding technique, in: 7th Computational Fluid Dynamics Conference, Cincinnati, OH, AIAA-1985-1523, 1985.
https://doi.org/10.2514/6.1985-1523

[3] R. Steijl and G. Barakos, Sliding mesh algorithm for CFD analysis of helicopter rotor–fuselage aerodynamics, International Journal for Numerical Methods in Fluids, vol. 58, issue 5, pp. 527-549, Feb. 2008.

https://doi.org/10.1002/fld.1757

[4] T. Renaud, A. Le Pape and C. Benoit, Unsteady Euler and Navier–Stokes computations of a complete helicopter, in Proc. 31st European Rotorcraft Forum, Florence, Italy, 2005. pp. 099.2-099.13.

[5] W. Khier, T. Schwarz and J. Raddatz, Time-accurate simulation of the flow around the complete BO105 wind–tunnel model, in: Proc. 31st European. pp. 87-1

[6] M. Bhagwat, A. Dimanlig, H. Saberi, E. Meadwcroft, B. Panda and R. Strawn, CFD/CSD coupled trim solution for the dual-rotor CH-47 helicopter including fuselage modeling, in American Helicopter Society Specialists Conference on Aeromechanics, San Francisco, CA, 2008.

[7] M. Dietz, W. Khier, B. Knutzen, S. Wagner and E. Krämer, Numerical simulation of a full helicopter configuration using weak fluid–structure coupling, in Proc. 46th AIAA Aerospace Science Meeting, Reno, NV, AIAA-2008-01-07, p. 401.
https://doi.org/10.2514/6.2008-401

[8] W. Khier, M. Dietz, T. Schwarz, S. Wagner, Trimmed CFD simulation of a complete helicopter configuration, in Proc. 33rd European Rotorcraft Forum, Kazan, Russia, 2007.

[9] M. Biava, W. Khier, L. Vigevano, CFD prediction of air flow past a full helicopter configuration, Aerospace Science and Technology, vol. 19, issue 1, pp. 3–18, Jun. 2012.
https://doi.org/10.1016/j.ast.2011.08.007

[10] NASA, Navier Stokes Equations, National Aeronautics and Space Administration, 05 May 2015.

[11] R. S. Raja, Coupled fluid structure interaction analysis on a cylinder exposed to ocean wave loading, M.S. thesis in Solid and Fluid Mechanics, Chalmers University of Technology, Göteborg, Sweden, 2012.